An experimental and theoretical approach to phosphonodithioato complexes: molecular orbital analysis by hybrid-DFT and EHT calculations on *trans*-bis[*O*-alkyl-phenylphosphonodithioato]Ni^{II}, and vibrational assignments

M. Carla Aragoni, Massimiliano Arca, Francesco A. Devillanova, John R. Ferraro, Francesco Isaia, Francesco Lelj, Vito Lippolis, and Gaetano Verani

Abstract: The synthesis and the full spectroscopic characterization (FT-IR, FT-Raman, ^{31}P CP MAS NMR) of *trans*-bis[*O*-ethyl-phenylphosphonodithioato]Ni^{II} (**3**) are reported. On the basis of hybrid-Density Functional Theory (DFT) calculations and Extended Hückel Theory (EHT) calculations, performed on the simpler *trans*-bis[*O*-methyl-phenylphosphonodithioato]Ni^{II} (**2**) model complex, the electronic structures of phosphonodithioato complexes in their ground states are fully described, and in particular the vibrational features are deeply analyzed, allowing an unprecedented insight into the vibrational features of *trans*-bis-*O*-methyl-phenylphosphono- and *trans*-bis(isopropylamidophosphono)-dithioato complexes of nickel(II), palladium(II), and platinum(II).

Key words: phosphonodithioato complexes, IR, Raman, DFT calculation.

Résumé : On rapporte la synthèse et la caractérisation spectroscopique complète (FT-IR, FT-Raman, ^{31}P CP MAS RMN) du *trans*-bis[*O*-éthyl-phénylphosphonodithioato]Ni^{II} (**3**). Sur la base de calculs de densité fonctionnelle hybride (DFT) et de calculs de Hückel étendus effectués (EHT) sur le complexe modèle plus simple, *trans*-bis-[*O*-méthyl-phénylphosphonodithioato]Ni^{II} (**2**), on présente une description complète des structures électroniques des complexes phosphonodithioato dans leurs états fondamentaux et, en particulier, on a analysé en détail les caractéristiques vibrationnelles ce qui permet d'obtenir une vue sans précédent des caractéristiques vibrationnelles des complexes *trans*-bis-*O*-méthyl-phénylphosphono- et *trans*-bis(isopropylamidophosphono)-dithioato du nickel(II), du palladium(II) et du platine(II).

Mots clés : complexes phosphonodithioato, IR, Raman, calculs DFT.

[Traduit par la Rédaction]

Introduction

Many reports have been published on the syntheses, characterizations, and reactivities of phosphoro- (1) and phosphinodithioates (2), since these compounds and their metal complexes have found wide application in industrial and agricultural fields (3), e.g., additives to lubricant oils (4), extraction reagents for metals (3, 5), flotation agents for mineral ores, and insecticides, rodenticides, and pesticides (3, 6). However, the chemistry of phosphono- and amido-phosphonodithioates has been only scarcely investigated, probably because of synthetic difficulties (7). Recently (8), we have reported a novel synthetic route to the preparation of square-planar metal-phosphonodithioates deriving from Lawesson's Reagent (LR, 2,4-bis(4-methoxy-phenyl)-[1,3,2,4]-dithiadiphosphetane-2,4-disulfide (**1**), see Scheme 1) (9), mainly known as thionation agent. First, these complexes were obtained as by-products in the synthesis of a new class [M(R,R′timdt)$_2$] (M = Ni, Pd, Pt; R,R′timdt = monoreduced form of disubstituted imidazolidine-2,4,5-trithione) of neutral metal-dithiolenes (10, 11), obtained by sulphuring disubstituted imidazolidine-2-thione-4,5-diones with **1** in the presence of a suitable metal powder or salt and of an alcohol, used because of solubility reasons (8). More generally, **1** was proved to react with nucleophilic alcohols (ROH) and amines (R′NH$_2$) to induce the opening of the P$_2$S$_2$ tetra-atomic ring, yielding phosphonodithioato and amidophosphonodithioato anions. Furthermore, their reaction with Ni^{II},

Received March 7, 2001. Published on the NRC Research Press Web site at http://canjchem.nrc.ca on October 12, 2001.

M.C. Aragoni, M. Arca, F.A. Devillanova, F. Isaia, V. Lippolis, and G. Verani.[1] Dipartimento di Chimica Inorganica ed Analitica, S.S. 554 bivio per Sestu, I-09042 Monserrato – Cagliari, Italy.
J.R. Ferraro. Chemistry and Materials Science Division, Argonne National Laboratory, 9700 Soth Cass Avenue, Argonne, Illinois 60439.
F. Lelj. Dipartimento di Chimica, Via N. Sauro 85, I-85100, Potenza, Italy.

[1] Corresponding author (telephone: +39-070-675-4474; fax: +39-070-675-4456; e-mail: verani@unica.it).

DOI: 10.1139/cjc-79-10-1483

Pd^{II}, and Pt^{II} salts (MCl_2 for M = Ni, Pd; K_2MCl_4 for M = Pd, Pt) gives the corresponding phosphono- and amidophosphono-dithioato complexes (12). These can also be obtained in a one-pot reaction by reacting **1** and the metal salts in the presence of the nucleophilic reagent. This route proved to be particularly well-suited for the synthesis of phosphonodithioato complexes deriving from light alcohols, since these can be used directly as solvents (8). Pursuant to our interest in this field, to understand the electronic and spectroscopic features of dithiophosphonato complexes, calculations based on Density Functional Theory (DFT) (13) have been performed on *trans*-bis[*O*-methyl-phenylphosphonodithioato]Ni^{II} (**2**, Scheme 1), chosen as a model compound. In fact, DFT calculations are assuming a primary role, since they give reliable results with inorganic compounds containing transition metals (11, 14) in their ground or excited states (15). With this in view, we have prepared *trans*-bis[*O*-ethyl-phenylphosphonodithioato]Ni^{II} (**3**), starting from 2,4-diphenyl-[1,3,2,4]-dithiadiphosphetane-2,4-disulfide (**4**). Complex **3** was previously reported, but only the cell constants and an average Ni—S distance were published (16, 17).

Results and discussion

Molecular orbital analysis

The geometry optimization of *trans*-bis[*O*-methylphenylphosphonodithioato]Ni^{II} (**2**, see Scheme 1) has been performed starting from the structural data determined by X-ray diffraction on *trans*-bis[*O*-ethyl-(4-methoxyphenyl)phosphonodithioato]Ni^{II} (**5**) and has correctly led to a square-planar coordination of the central metal ion, with the phosphorus atoms slightly out of the coordination plane (Fig. 1). In Table 1, a comparison between the calculated bond distances and angles and those measured by X-ray diffraction on **5** (8) (where the phenyl is replaced by a *p*-methoxyphenyl) and *trans*-bis[isopropylamido-(4-methoxyphenyl)phosphonodithioato]Ni^{II} (**9**) (where the ethoxy group is replaced by an isopropylamine moiety) (12) is reported. As found in the case of other hybrid-DFT calculations on Ni complexes deriving from sulphured ligands (8, 11), the metal—sulphur distances are slightly overestimated (a distance of 2.278 Å has been calculated, compared to an average value of 2.20 Å found experimentally) (17), while the remaining calculated bond distances and angles are similar to the experimental ones reported for **5** (8) and *trans*-bis[(4-methoxyphenyl)-*O*-methyl-phosphonodithioato]M^{II} (M = Pd (**7**) and Pt (**8**)) complexes (12).[2] Some differences regarding the orientation of the substituents to the phosphorus atom [S(1,2)-P(2)-O(1), S(1,2)-P(1)-C(2), P(1)-O(1)-C(1)] should be attributed to crystal packing effects. The comparison can also be extended to the reported structures of the Pd^{II} and Pt^{II} analogues of **2**, where values similar to those reported for **5** and **9** were found (17). To qualitatively understand the interactions between the atomic orbitals (AO's) of the Ni^{II} ion and the molecular orbitals (MO's) of the two ligand units, the Fragment Molecular Orbitals (FMO) approach within the Extended Hückel Theory (EHT) is employed. In Fig. 2 an interaction diagram showing the orbitals, whose eigenvalues lay in the range between –8 and –15 eV, is reported. In the idealized molecular C_{2h} point group the five 3*d* AO's span in three a_g ($d_{x^2-y^2}$, d_{z^2}, d_{xy}) and two b_g (d_{xz}, d_{yz}) representations. The 21a_g highest occupied molecular orbital (HOMO) of **2** is a π-MO largely made up of the $d_{x^2y^2}$ AO (25%), which is raised in energy by the antibonding interaction with the 21a_g FMO of the ligands, constituted by a combination of sulphur 3*p* AO's perpendicular to the coordination plane. The interaction between the 14b_g FMO of the ligands (in plane sulphur *p* AO's) with the d_{xz} and d_{yz} AO's (25 and 16%, respectively) origins the σ-type 14b_g lowest unoccupied molecular orbital (LUMO). This MO happens to lay at roughly the same energy as three other nonbonding MO's (22a_g, 19b_u, 13a_u), which are π-orbitals arising from the combinations of the 2*p* AO's of the aromatic carbon atoms. The HOMO-1 13b_g also contains a contribution of Ni AO's (namely d_{yz} and d_{xz}, 25 and 15%, respectively) π-interacting with a b_g combination of 3*p* sulphur AO's. Metal *d* AO's also contribute to other MO's at lower energies, such as 20a_g (49% d_{z^2}, 16% d_{xy}), 18 a_g (32% $d_{x^2-y^2}$, 2% d_{z^2}, 11% d_{xy}), 15a_g (2% d_{z^2}, 8% d_{xy}), and 7b_g (28% d_{xz}).

Vibrational assignments

The calculation of harmonic frequencies from DFT energy gradients allows one to verify the optimized geometry and to obtain an unprecedented insight into the vibrational spectra of such complexes (Tables 2–4). Only two negative frequency values have been calculated (–84 and –82 cm^{-1}), which are related to rotations of methyl and phenyl groups, and therefore, are due to the presence of a constrained inversion center. A first examination of the simulated spectra (Fig. 3) shows that the use of transferable scaling factors (18), depending on the nature of the single vibrations, gives better results compared to uniform scaling factors. In this case, the slight differences found between the calculated and the experimental bond lengths and angles force the use of scaling factors that are quite different from unity, because of the unharmonic nature of the experimental vibrations. In general, scaling factors have been obtained by comparing the calculated harmonic frequency values to those measured for **3** and *trans*-bis[(4-methoxyphenyl)-*O*-methylphosphonodithioato]Ni^{II} (**6**), depending on the group involved in the vibrations. Because of the presence of an inversion centre, the IR spectra are expected to show only the

---

[2] To ascertain if the differences between the calculated and the experimental bond lengths and angles were to be attributed to the hybrid nature of the functional B3LYP, geometry optimization followed by frequency calculations have been performed with the same basis set on the simplified *trans*-bis[*O*-methyl-methylphosphonodithioato]Ni^{II} model complex, with three different functional, namely BLYP, BPW91, and B3LYP. Both the calculated geometries and frequencies are similar in the three cases. As regards the $(PS_2)_2Ni$ local moiety, the bond distances and angles calculated for the model complex are very similar to those calculated for **2** (Table 1). Although the BPW91 functional slightly reduces the overestimation of the Ni—S bond distances (2.282, 2.249, 2.278 Å for BLYP, BPW91, and B3LYP), it tends to calculate elongated P—S (2.044, 2.025, 2.020 Å for BLYP, BPW91, and B3LYP), P—O (1.656, 1.652, 1.628 Å for BLYP, BPW91, and B3LYP), and P—C (1.849, 1.836, 1.829 Å for BLYP, BPW91, and B3LYP) distances, compared to the experimental average values determined for **5** (Table 1). As regards frequency calculations, the results are also pretty similar, since the three functionals calculated the same number of bands in the same order, BLYP functional leading to smaller absolute wavenumber values.

Scheme 1.

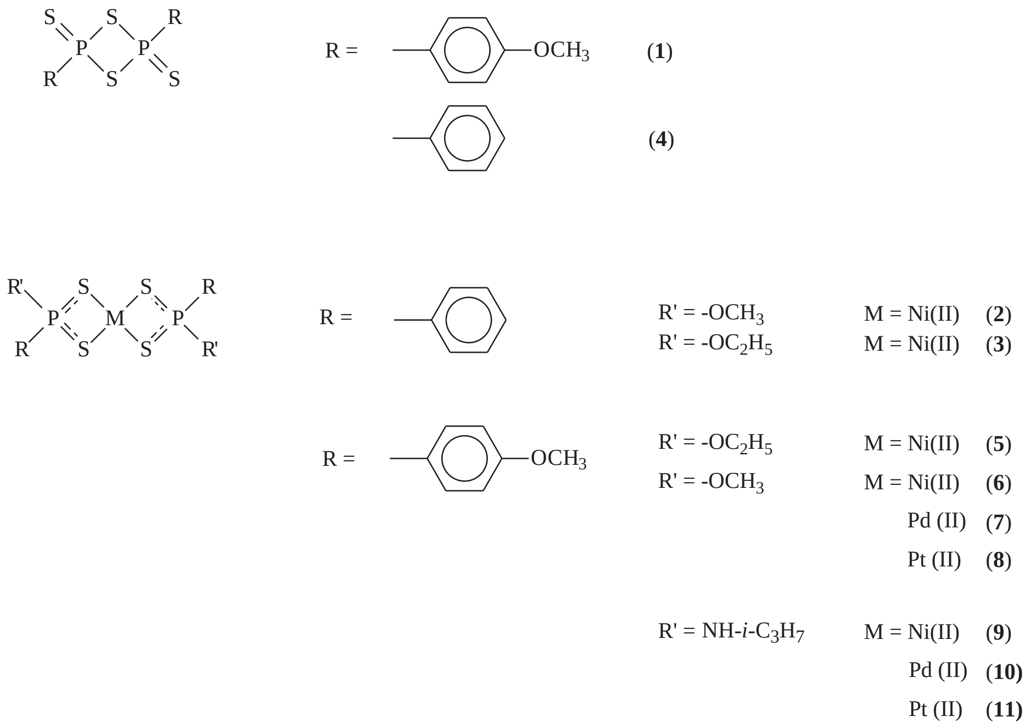

Fig. 1. Atom numbering scheme for model complex **2**.

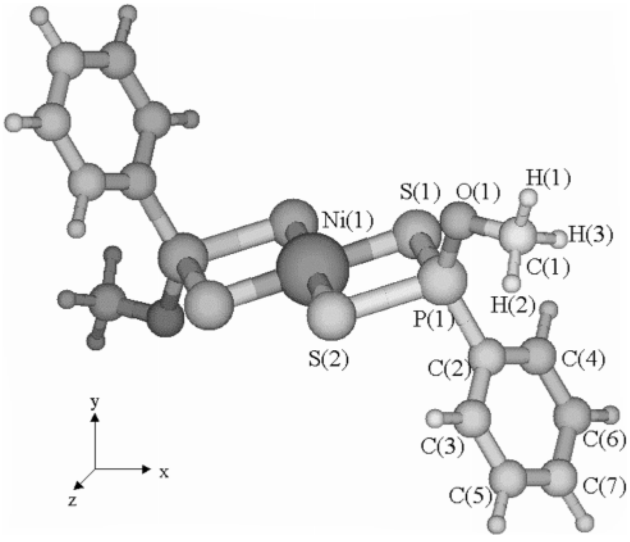

Table 1. Selected optimized bond lengths (Å), angles (°), and dihedral angles (°) for model complex *trans*-bis[*O*-methylphenylphosphonodithioato]Ni^{II} (**2**) compared with average values measured on analogue Ni complexes **5** and **9**.

	2	**5**[a]	**9**[a]
Bond lengths (Å)			
Ni(1)—S(1,2)	2.278	2.221	2.223
P(1)—S(1,2)	2.020	1.994	2.015
P(1)—O(1)	1.631	1.580	—
P(1)—C(2)	1.823	1.782	1.795
O(1)—C(1)	1.437	1.456	—
Bond angles (°)			
S(1)-Ni(1)-S(2)	88.086	88.14	87.64
S(1)-Ni(1)-S(1′)[b]	91.914	91.86	92.81
Ni(1)-S(1,2)-P(1)	80.498	83.78	84.96
S(1)-P(1)-S(2)	103.264	101.57	99.67
S(1,2)-P(1)-C(2)	112.140	113.94	112.67
S(1,2)-P(1)-O(1)	111.642	114.09	—
O(1)-P(1)-C(2)	106.160	99.85	—
P(1)-O(1)-C(1)	125.218	120.9	—

[a] Average values. Supplementary materials of refs. 8 and 12.

[b] Symmetry transformation used to generate (′): –*x*, –*y*, –*z*.

antisymmetric modes, and the Raman spectra only the symmetric ones. At any rate, as far as the ligand units are concerned, for each mode, two combinations (symmetric and antisymmetric) are possible, among which the symmetric combinations appear in the Raman spectra and the antisymmetric ones in the IR spectra. Since the two ligand groups are independent, the two combinations are almost degenerate in energy. Therefore, symmetric vibrational modes related to the two ligand units appear in the IR spectra through their antisymmetric combinations, as well as symmetric coupling of antisymmetric vibrations are Raman active.

An examination of the vibrational frequencies calculated for **2** shows that the bands having the highest energies can be found in the region 3100–2900 cm^{-1} (Table 2). In this region the symmetric and antisymmetric C—H stretching normal modes are calculated, and can be found in all the dithiophosphonato complexes, with minor differences due to the nature of the substituents.

Below 1600 cm^{-1}, the first band found in the FT-IR and Raman spectra of **6** is a strong peak at 1597 and 1590 cm^{-1}, respectively, sided by a less intense peak falling at 1567 cm^{-1} in both spectra. These peaks correspond to the two possible

Fig. 2. Qualitative EHT–FMO interaction diagram between the Ni^{II} $3d$ atomic orbitals (right side) and the ligand molecular orbitals (left side) in model complex **2**. FMO labelling refers to the C_{2h} point group. Molecular orbitals are connected to FMO's contributing for at least 20%.

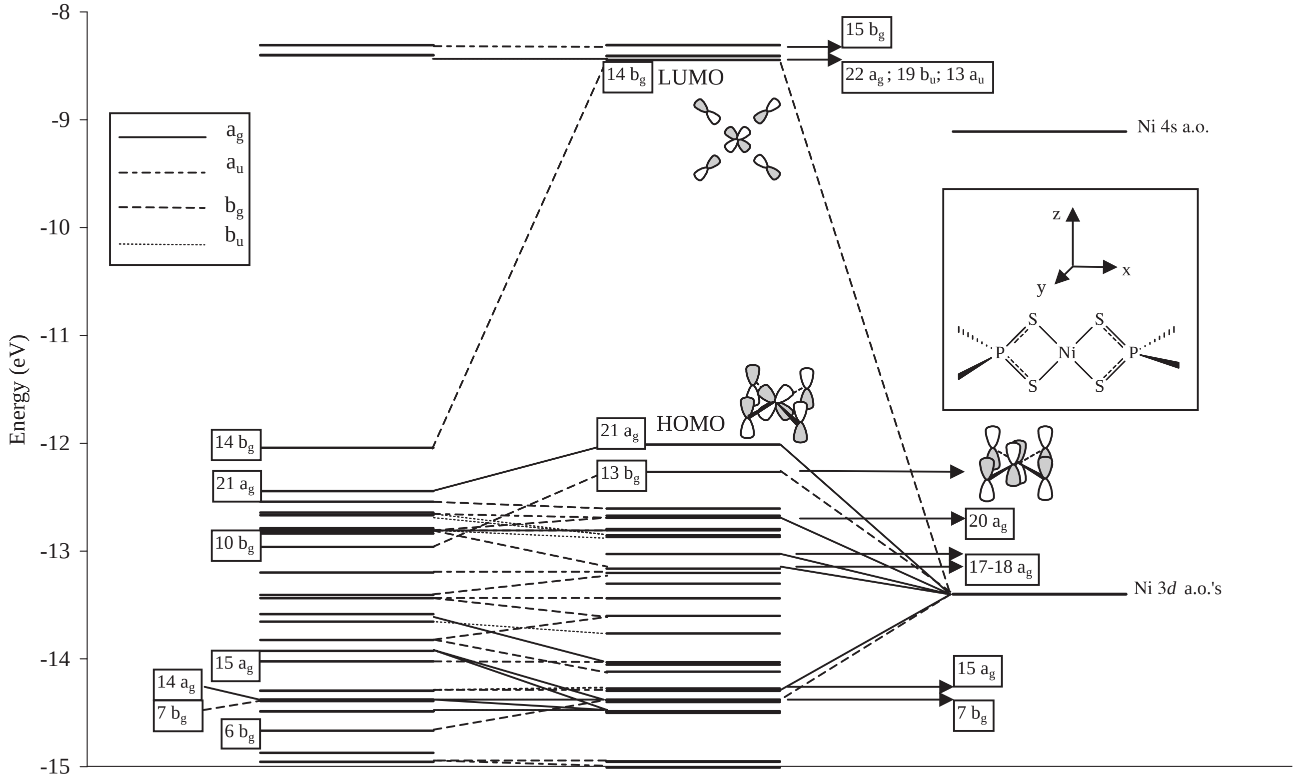

Table 2. Selected calculated scaled and unscaled harmonic frequencies (cm^{-1}), scaling factors, reduced masses (amu), calculated IR intensities ($km\ mol^{-1}$), and normal mode descriptions for model complex **2**, and corresponding FT-IR and FT-Raman (italics) experimental bands (cm^{-1}) for complexes **3** and **6**, in the region 3300–3000 cm^{-1}.

Unscaled freq. (cm^{-1})	Scaling factor	Scaled freq. (cm^{-1})	Reduc. mass (amu)	IR int. ($km\ mol^{-1}$)	Exp. freq. **3** (cm^{-1})	Exp. freq. **6** (cm^{-1})	Normal mode description
3216	0.96	3088	1.098	45.7	3084 (vw)	3088 (vw)	Symmetric stretching C(3–7)—H
3211	0.96	3082	1.094	20.6			Antisymmetric stretching C(4–6)—H
3205	0.96	3076	1.091	14.3	3070 (vw)	3075 (vw), *3074*	Stretching C(3,4,7)—H
3197	0.96	3069	1.088	12.4			Antisymmetric stretching C(3–6)—H
3188	0.96	3060	1.085	0.1	*3053*		Symmetric stretching C(5–7)—H
3166	0.96	3040	1.106	40.0			Symmetric stretching C(1)—H(1,2 in phase; 3 out of phase)
3140	0.96	3015	1.108	34.5	2975 (mw)	2972 (w), *2973*	Antisymmetric stretching C(1)—H(2,3)
3064	0.96	2941	1.030	122.8	2930 (w), *2930*	2941 (mw), *2943*	Symmetric stretching C(1)—H

Note: In this region calculated symmetric and antisymmetric modes fall at the same frequencies.

combinations of ν_s and ν_{as} C—C stretching of the phenyl rings, and are very weak in the FT-IR spectrum of **3** (IR: 1585 and 1571 cm^{-1}; Raman: only 1586 cm^{-1}). In the simulated spectrum of **2** (Table 3) these two bands are also calculated to be very weak (2.2 and 0.5 $km\ mol^{-1}$, respectively). Therefore, this suggests that the presence of the methoxy substituent in the *para* position of the phenyl ring causes an enhancement in the intensity of the bands in the IR spectra, which is presumably due to the negative charges on the oxygen atoms, which enhance the variation in the dipole mo-

Table 3. Selected calculated scaled and unscaled harmonic frequencies (cm^{-1}), scaling factors, reduced masses (amu), calculated IR intensities (km mol^{-1}), and normal mode descriptions for model complex **2**, and corresponding FT-IR and FT-Raman (italics) experimental bands (cm^{-1}) for complexes **3** and **6**, in the region 1700–500 cm^{-1}.

Unscaled freq. (cm^{-1})	Scaling factor	Scaled freq. (cm^{-1})	Reduc. mass (amu)	IR int. (km mol^{-1})	Exp. freq. **3** (cm^{-1})	Exp. freq. **6** (cm^{-1})	Normal mode description
1647	0.96	1585, *1585*	5.250, *5.245*	2.2	1585 (w) *1586*	1597 (vs) *1590*	Symmetric stretching C(3,4)—C(5,6)
1632	0.96	1571, *1571*	5.138, *5.135*	0.5	1571 (w)	1567 (mw), *1566*	Antisymmetric stretching C(2,6)—C(3,7)
1530	0.95	1454, *1454*	1.927, *1.930*	8.8	1466 (mw)	1465 (mw)	Symmetric bending C(3–6)—H
1525	0.95	1449, *1449*	1.048	20.6	1449 (w), *1450*	1454 (mw), *1454*	Rocking C(1)—H(1–3)
1522	0.95	1446, *1446*	1.073, *1.072*	37.8			Scissoring C(1)—H(2,3)
1501	0.95	1426, *1426*	1.129	10.7	1436 (ms)	1426 (w), *1424*	Wagging C(1)—H(2,3)
1482	0.95	1408, *1408*	2.117	32.1	1389 (m), *1389*	1407 (mw)	Antisymmetric stretching C(3,4)—C(5,6) + symmetric bending C(5–7)—H
1365	0.95	1297, *1297*	1.914, *1.913*	10.2	1308 (mw)	1307 (ms), *1307*	Antisymmetric stretching C(2,6)—C(3,7) + bending C(3,4,7)—H
1332	0.95	1265, *1265*	2.718, *2.720*	5.6	1284 (vw), *1282*	1294 (s), *1294*	Stretching C(2)—C(3,4) + bending C(3–6)—H
1219	0.97	1182, *1182*	1.151	17.7	1182 (mw), *1184*	1186 (sh), *1175*	Symmetric bending C(3,4)-C(5,6)-H + bending C(5,6)-C(3,4)-H
1199	0.97	1165, *1165*	1.303, *1.304*	20.5	1157 (m), *1158*	1165 (m)	Out of plane wagging C(1)—H(2,3) + bending O(1)-C(1)-H(1)
1121	0.99	1113, *1113*	2.959	105.6	1113 (vs), *1113*	1118 (vs), *1118*	Stretching C(2)—P(1)
1112	0.99	1101, *1101*	1.630	2.9	1101 (sh)	1108 (sh)	Antisymmetric stretching C(3,4)—C(5,6) + bending CH aromatic
1074	0.93	1003	7.132	1018.7	1014 (vs)	1003 (vs)	Stretching O(1)—C(1)
1081		1005	7.263	—	*1027*	*1005*	
1054	1.00	1054, *1054*	2.907, *2.898*	2.7			Phenyl ring breathing
1014	1.00	1014, *1014*	5.494, *5.458*	5.4	*998*	1011 (sh)	Phenyl ring breathing C(3,4,7)
749	1.00	749	4.173	413.0	783 (s)	789 (vs)	P(1)—O(1) + deforming out of plane CH aromatic
752		752	3.094	—		*801*	
725	1.00	725	7.403	119.3			Breathing phenyl rings
726		726	7.342	—			
703	1.00	703, *703*	2.510, *2.491*	38.8			Deforming out of plane C(3,4,7)—H
657	0.96	631	21.853	103.3	627 (s)	622 (ms)	Antisymmetric stretching P(1)—S(1,2)
645		619	15.258	—	*623*	*618*	
627	1.00	627	6.893	11.9			Breathing phenyl rings
625		625	7.974	—			
582	0.96	559	11.950	224.4	565 (vs)	550 (s)	Symmetric stretching P(1)—S(1,2) + stretching P(1)—C(2)
583		560	11.804	—	*566*	*553*	

ments. Many differences can be found in the vibrational spectra of **3** and **6** in the region of 1500–1400 cm^{-1}. In particular, four normal modes are calculated to be IR-active and they fall at 1449, 1446, 1426, and 1408 cm^{-1}: the first two are due to rocking and scissoring modes of the methyl groups, the third to an umbrella wagging of the methyl

Table 4. Selected calculated scaled and unscaled harmonic frequencies (cm^{-1}), scaling factors, reduced masses (amu), calculated IR intensities (km mol^{-1}) and normal mode descriptions for model complex **2**, and corresponding FT-IR and FT-Raman (italics) experimental bands (cm^{-1}) for complexes **3** and **6**, in the region 500–50 cm^{-1}.

Unscaled freq. (cm^{-1})	Scaling factor	Scaled freq. (cm^{-1})	Reduc. mass (amu)	IR int. (km mol^{-1})	Exp. freq. **3** (cm^{-1})	Exp. freq. **6** (cm^{-1})	Normal mode description
498	1.00	498	4.339	19.6			Out of plane phenyl ring deforming
499		499	4.354	—		*491*	
395	1.10	435	12.401	39.4	470 (ms)	435 (m)	Bending S(1)-Ni-S(2)
401		442	12.842	—	*470*	*440*	
336	1.12	375	5.769	8.9	375 (mw)	375 (m)	Bending P(1)-O(1)-C(1) + twisting phenyl ring
337		378	5.895	—	*386*	*375*	
327	1.10	360	1.788	3.9			Bending S(1)-Ni(1)-S(1)′
320	0.96	360	8.700	—			Symmetric wagging P(1)—O(1),C(2)
319	1.10	351	28.800	79.5	354 (s)	351 (m)	Antisymmetric stretching Ni—S(1,2)
313	1.10	344	27.979	1.9		*343*	Antisymmetric stretching Ni—S(1,2)
294	1.10	323	11.266	—	*308*	*314*	Symmetric stretching Ni—S(1,2) + S(1)-P(1)-S(2) bending + P(1)-O(1)-C(1) bending
259	1.07	277	5.341	29.6		277 (mw)	Bending P(1)-O(1)-C(1) + S(1)-P(1)-S(2)
248	1.10	273	15.680	—	*273*	*278*	Antisymmetric stretching Ni—S(1,2)
244	1.10	268	5.410	—			Symmetric Ni(1)—S(1,2) + bending P(1)-O(1)-C(1)
211	1.10	232	12.968	19.9	204 (mw)	202 (w)	Symmetric stretching Ni(1)—S(1,2) + bending S(1)-P(1)-S(2)
206	1.10	226	8.324	2.1			Bending S(1)-Ni(1)-S(1)′ + twisting O(1)-P(1)-C(2)
136	1.10	150	9.157	—	*142*	*137*	Symmetric breathing P(1)-S(1,2)-Ni(1)
133	1.10	147	11.898	1.8			NiS_4 out of plane deforming
118	1.00	118	1.417	—		*116*	Methyl group rotation
113	1.00	113	4.150	—	*113*	*102*	Methyl group rotation + twisting NiS_4
91	1.00	91	4.859	—	*86*	*84*	NiS_4P_2 ring deformation

group, and the fourth to a combination of C—C stretching and C-C-H in plane bending of the phenyl rings. Since the first two modes are almost degenerate in frequency, these four normal modes result in three bands in the simulated spectrum. The first and the third bands are found in the FT-IR spectrum of **3** at 1436 (the shift due to the presence of an ethyl instead on a methyl group) and 1389 cm^{-1}, while the umbrella deformation is not found in **3**, since no OCH_3 group is present. With regards to **6**, the bands are more numerous due to the presence of another OCH_3 group, as a substituent, at the phenyl ring, whose C–H deformations should fall in the same region. Such deformations can be considered responsible for a very strong IR band at 1500 cm^{-1}, which is found almost identical in the corresponding complexes **7** and **8** (12), and in *trans*-bis[isopropylamido-(4-methoxyphenyl)-phosphonodithioato]M^{II} (M = Ni (**9**), Pd (**10**) and Pt (**11**)). This region of the vibrational spectrum shows only very weak bands in the Raman spectra of all compounds.

The bands between 1300 and 1100 cm^{-1} are attributed to vibrations mainly regarding bending modes of the bonds in the aromatic rings. Among them, the bands falling at 1182 and 1177 cm^{-1} in the FT-IR spectra of **3** and **6**, respectively (calculated at 1182 cm^{-1} for **2**), are also found with remarkable intensities in their symmetric combination in the Raman spectra (1184 and 1175 cm^{-1} in **3** and **6**, respectively). It is interesting to note that in this case the presence of the substitution in the phenyl ring also causes an increase in the intensities of the IR bands. Only the IR bands falling at 1113, 1113, and 1118 cm^{-1} (exactly the same values of the Raman peaks) in the simulated spectrum of **2** and in those of **3** and

Fig. 3. Simulated FT-IR spectrum based on calculated scaled harmonic frequencies for model complex **2**, experimental middle-IR (1700–450 cm^{-1}) and far-IR (450–50 cm^{-1}) spectra for complexes **3** and **6**. The bands corresponding to same normal modes are connected by dotted lines. Vertical arrows are related to bands involving the methoxy group bound to the phenyl ring in complex **6**.

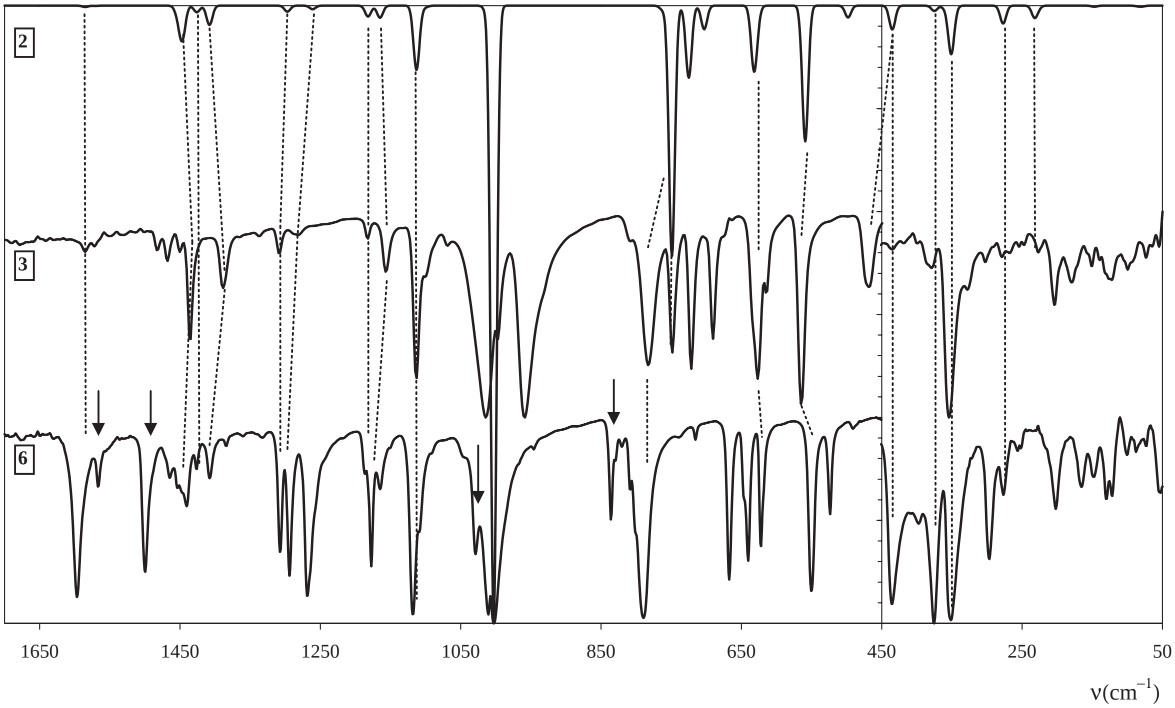

6, respectively, are strong, possibly because of the P—C stretching contribution to the vibrational mode. The most intense band in the whole simulated spectrum of **2** is found at 1003 cm^{-1} and is due to a pure (calculated reduced mass 7.1 amu) C—O stretching normal mode. This band in fact is found as a very strong IR peak both in **3** (1014 cm^{-1}) and in **6** (1003 cm^{-1}). The side band found in FT-IR spectrum of **5** at 1030 cm^{-1} is absent in **3** and can, therefore, be tentatively attributed to the C—O stretching vibration of the methoxy substituent at the phenyl ring. In fact, while the peak around 1000 cm^{-1} is absent in amidophosphonodithioato complexes **9–11**, the ν_{O-CH_3} vibration is found at 1020, 1019, and 1019 cm^{-1} for **9**, **10**, and **11**, respectively. In the Raman spectra of complexes **3** and **6**, the peak around 1000 cm^{-1} is strong only for **3**, while for **6** the band is weak.

In the FT-IR spectrum of **3** the strong peak found at 959 cm^{-1} (very weak in the Raman spectrum at 961 cm^{-1}) is absent in the calculated spectrum of **2**. Therefore, this band should be due to a vibrational mode of the ethoxy substituent, since it is also absent in **6** but present in **5** at 941 and 943 cm^{-1} in the FT-IR and Raman spectra, respectively. Conversely, in the FT-IR spectrum of **6**, the band at 836 cm^{-1} (Raman 839 cm^{-1}), absent in **3** and in the simulated spectrum of **2**, appears in all the vibrational spectra of compounds derived from **1** and, consequently, it might be due to another mode of the methoxy substituent at the phenyl.

Moving to lower frequencies, a very intense IR band is found at 783 and 789 cm^{-1} (786 and 801 cm^{-1} in the Raman spectra) for compounds **3** and **6**, respectively; this band can be correlated to the vibration calculated for **2** at 749 cm^{-1}, which is due to a combination of P—O stretching and C—H out of plane deforming of the phenyl ring. These vibrations, in the region between 750 and 500 cm^{-1} (fingerprint region), are mainly due to out of plane ring deforming of the phenyl moieties and to the P—S and P—O stretching modes. In particular, the band calculated at 631 cm^{-1} is attributed to the antisymmetric stretching of the P—S bonds and appears as an intense peak in all the vibrational spectra of all the synthesized complexes (**3**: 627 (IR), 623 (Raman) cm^{-1}; **5**: 623 (IR), 616 (Raman) cm^{-1}; **6**: 622 (IR), 618 (Raman) cm^{-1}; **7**: 611 (IR), 611 (Raman) cm^{-1}; **8**: 612 (IR), 612 (Raman) cm^{-1}; **9**: 608 (IR), 600 (Raman) cm^{-1}; **10**: 599 (IR), 596 (Raman) cm^{-1}; **11**: 598 (IR), 599 (Raman) cm^{-1}).

In the far-IR region (Table 4) the antisymmetric S-Ni-S bending appears at 470 and 435 cm^{-1} for **3** and **6**, respectively. This band, calculated at 435 cm^{-1} for **2**, depends strongly on the groups bound to the phosphorus atoms, and in fact varies by about 60 cm^{-1} on passing from phosphonodithioato (435, 431, 429 cm^{-1} for **6**, **7**, and **8**, respectively) to amidophosphonodithioato complexes (496, 497, 495 cm^{-1} for **9**, **10**, and **11**, respectively), while its position is virtually independent of the metal, indicating similar force constants for this bending mode. Therefore it is not surprising that the change of the alkoxy group determines a clear variation in the position of this band. Following the same trend found for the antisymmetric stretching, the symmetric one falls in the Raman spectra at 470 cm^{-1} for **3**, 440 cm^{-1} for **6**, 432 cm^{-1} for both **7** and **8**, and 463 cm^{-1} for **9**, **10**, and **11**. The antisymmetric metal—sulphur stretching is calculated at 351 cm^{-1} to be the most intense band in this region and is found at roughly the same frequency in the FT-IR spectra of both **3** and **6**. This band falls at 356, 314, and 308 cm^{-1} for compounds **9**, **10**, and **11**, respectively, and is found at 346, 316, and 303 cm^{-1} for **5**, **7**, and **8**, respectively. The symmetric Ni—S stretching, calculated at 323 cm^{-1}, is found in the FT-Raman spectra of all complexes: 308 (**3**), 311 (**5**), 314 (**6**), 326 (**7**), 316 (**8**), 313 (**9**), 327 (**10**), and 316 cm^{-1} (**11**), with the bands being shifted according to the ratio between the different metal–sulphur bond strength constants and the respective reduced masses. According to the previous assignments the symmetric stretching frequency is found at higher frequencies compared to the unsymmetric ones for nickel-complexes **3**, **5**, **6**, and **9**, as well as in the calculated spectrum of **2**. Surprisingly, in the case of Pd and Pt complexes **7**, **8**, **10**, and **11** this trend is inverted. Another band, calculated at 358 cm^{-1} as a symmetric combination of torsions around the P atoms, can be found in the Raman spectra at 343 (**6**), 342 (**7**), 342 (**8**), 342 (**9**), 344 (**10**), and 345 cm^{-1} (**11**). This band becomes weaker in the case of **3** and **5** (340 and 344 cm^{-1}, respectively). Finally, in the lowest frequency region of the far-IR and Raman spectra the bands are originated by deforming of the metallacycle PS_2Ni ring and by alkoxy group rotations.

Conclusions

The synthesis of *trans*-bis[*O*-ethyl-phenylphosphonodithioato]Ni^{II} (**3**) confirms the reactivity of substituted [1,3,2,4]-dithiadiphosphetane-2,4-disulfides towards nucleophilic reagents, previously explored by us on commercially available Lawesson's Reagent (**1**). The complex has been fully characterized by spectroscopic techniques. At any rate, the most interesting results come from an examination of the DFT-calculated vibrational frequencies, which allows us to deeply investigate not only the FT-IR and FT-Raman spectra of **3**, but also those of other phosphono- (**6**–**8**) and amidophosphono-dithioato (**9**–**11**) complexes previously reported by us.

Experimental

All the reagents and solvents were purchased from Aldrich or Merck and were used without further purification. Elemental analyses were performed with an EA1108 CHNS-O Fisons instrument. Fourier transform infrared spectra (FT-IR) were recorded on a Bruker IFS55 spectrometer at room temperature using a flow of dried air. Far-IR (500–50 cm^{-1}) spectra (resolution 2 cm^{-1}) were recorded as polythene pellets with a Mylar beam-splitter and polythene windows. Middle IR spectra (resolution 2 cm^{-1}) were recorded as KBr pellets, with a KBr beam-splitter and KBr windows. FT-Raman spectra were recorded with a resolution of 2 cm^{-1} on a Bruker RFS100 FT-Raman spectrometer, fitted with an In-Ga-As detector (room temperature) operating with a Nd-YAG laser (excitation wavelength 1064 nm) with a 180° scattering geometry. Solid state ^{31}P CP MAS NMR spectra were recorded on a Varian Unity Inova 400 MHz instrument operating at 161.9 MHz with samples packed into a zirconium oxide rotor. The ^{31}P NMR chemical shifts were calibrated indirectly through the H_3PO_4 85% peak (δ 0.0). Quantum-chemical calculations were performed using the commercially available suite of programs Gaussian 98 package (19). Density Functional Calculations (DFT) (13) were performed on **2** using the hybrid B3LYP functional (which uses a mixture (20) of Hartree-Fock and DFT exchange along with DFT correlation: the Lee–Yang–Parr correlation functional (21) together with the Becke's gradient correction) (22).[3] The 6–31G(*d*) basis sets (23) were employed throughout. Integration was performed numerically using a total of 7500 points for each atom (Ultrafinegrid option). Starting from geometrical parameters determined for **5** (8), and avoiding introduction of any geometrical constraints but the inversion centre, a geometry optimization was performed and the results of the calculations were examined with the Molden 3.6 program (24). The optimized structure was verified by normal-mode harmonic frequency analysis. Harmonic frequencies were obtained using the second derivatives of the DFT energy, computed by numerical differentiation of the DFT energy gradients. Calculated harmonic frequencies were extracted from the output file and converted in a simulated spectrum with the Tabfreq program after application of the scaling factors, using DFT-calculated intensities and a halfbandwidth of 10 cm^{-1}. According to a referee suggestion, the computational results[2], both the geometry optimization and the frequency calculations, have been repeated on the simpler *trans*-bis[*O*-methyl-methylphosphonodithioato]Ni^{II} model complex, using BLYP, BPW91, and B3LYP functionals and the same 6–31G(*d*) (23) basis set for all atoms. The first two functionals are pure-DFT functionals, combining the Becke's (25) 1988 exchange functional with the Lee et al.'s (including both local and nonlocal terms) (26), and Perdew and Wang's (27) 1991 gradient-corrected correlation functionals, respectively. The qualitative MO analyses have been obtained by means of Extended Hückel Theory (EHT) (28) using the CACAO (Computer Aided Composition of Atomic Orbitals) program package (29) on the hybrid-DFT optimized geometry, regularized to obtain an idealized C_{2h} symmetry. The interaction diagram was generated using the fragment molecular orbital (FMO) approach (30). Parameters used in EHT calculations were taken from the standard database of CACAO.

Synthesis of 2,4-diphenyl-[1,3,2,4]-dithiadiphosphetane-2,4-disulfide (4)

Compound **4** was synthesized according to literature methods (31), by reacting $(PhP)_3S_3$ with an excess of elemental sulphur in carbon disulfide.

Synthesis of $C_{16}H_{20}O_2P_2S_4Ni$ (3)

An excess of $NiCl_2 \cdot 6H_2O$ was reacted with **4** (2.7 g, 8 mmol) in absolute ethyl alcohol solution (100 mL). The filtered solid was recrystallized from CH_2Cl_2–EtOH (1:1 v/v) solution. Yield: 3.56 g, 7.2 mmol, 90%; mp 179°C. FT-IR (3500–450 cm^{-1} KBr; 450–50 cm^{-1} polythene) (cm^{-1}): 3050 (vvw), 3020 (vvw), 2975 (mw), 2930 (w), 2896 (w), 2857 (vvw), 1585 (w), 1571 (vw), 1481 (vw), 1468 (mw), 1449 (w), 1436 (ms), 1389 (m), 1307 (w), 1309 (w), 1282 (vw), 1182 (mw), 1157 (m), 1113 (vs), 1069 (w), 1014 (vs),

---

[3] Gaussian 98 *z*-matrix input and output file, optimized cartesian coordinates of atoms in complex **2**, list of unscaled calculated harmonic frequencies, IR activity, reduced mass, force constants, and atom displacements for each calculated vibration are available from author on request.

997 (ms), 959 (vs), 783 (s), 748 (s), 721 (s), 690 (ms), 627 (s), 614 (m), 565 (vs), 468 (m), 469 (m), 435 (vw), 416 (vw), 379 (w), 354 (vs), 302 (w), 279 (w), 254 (w), 227 (w), 204 (m), 179 (mw), 151 (w), 122 (mw), 99 (w), 73 (w), 55 (w). FT-Raman (solid state; in parethesis intensities scaled on the highest peak taken equal to 10.0 are reported): 3053 (3.6), 2966 (0.9), 2930 (0.9), 2919 (0.8), 2989 (0.4), 1586 (2.7), 1440 (0.5), 1158 (0.9), 1113 (2.2), 1027 (0.9), 998 (5.4), 623 (1.7), 566 (6.0), 470 (0.9), 386 (0.8), 308 (4.5), 273 (2.5), 2.42 (4.0), 142 (7.8), 114 (10.0), 86 (9.1) cm^{-1}. ^{31}P CP MAS NMR δ: 108.2, 106.9. Anal. calcd. for $C_{16}H_{20}O_2P_2S_4Ni$: C 39.0, H 4.1, S 26.0; found C 39.1, H 4.4, S 25.6.

*Synthesis of complexes **5–11***

The syntheses of compounds **5–11** were accomplished as previously reported (8, 12).

Acknowledgments

We thank the Consorzio interuniversitario per le Applicazioni di Supercalcolo per Università e Ricerca (CASPUR) and Dr. Nico Sanna for hosting the calculations on **2**, the Consorzio Interuniversitario del Nord Est Italiano per il Calcolo Automatico (CINECA) for hosting calculations on *trans*-bis[*O*-methyl-methylphosphonodithioato]Ni^{II} model complex, and the Regione Autonoma della Sardegna and MURST (Ministero dell'Università e della Ricerca Scientifica) for financial support.

References

1. J.R. Wasson, G.M. Woltermann, and H.J. Stoklosa. Forstschr. Chem. Forsch. (Topics Curr. Chem.) **35**, 65 (1973).
2. W. Kuchen and H. Hertel. Angew. Chem. Int. Ed. Engl. **8**, 89 (1969).
3. (*a*) H. So, Y.C. Lin, G.S. Huang Gibbs, and S.T. Chang. Terny. Wear, **166**, 17 (1993); (*b*) V.V. Mikhailov, Yu V. Kokhanov, K. Kazaryan, E.N. Matreeva, and A. Kozodoi. Plast. Massy, **9**, 23 (1970); (*c*). M. Fuller, M. Kasrai, J.S. Sheasby, G.M. Bancroft, K. Fyfe, and K.H. Tan. Tribol. Lett. 367 (1995).
4. (*a*) P.G. Harrison, M.J. Begley, T. Kikabhai, and F. Killer. J. Chem. Soc. Dalton Trans. 925 (1986); (*b*) Y. Lin. Lubr. Eng. **51**, 855 (1995); (*c*) A.J. Burn, I. Gosney, C.P. Warrens, and J.P. Wastle. J. Chem. Soc. Perkin Trans. 2, 265 (1995); (*d*) E.S. Yamaguchi and P.R. Ryason. Tribol. Test, **3**, 123 (1996); (*e*) S. Contarini, G. Tripaldi, G. Ponti, S. Lizzit, A. Baraldi, and G. Paolucci. Appl. Surf. Sci. **108**, 359, (1997); (*f*) B. Chen, J. Song, Y. Ye, and J. Dong. Tribologia, **29**, 207 (1998); Chem. Abst. 129:218 781.
5. R.C. Mehrotra, G. Srivastava, and B.P.S. Chauhan. Coord. Chem. Rev. **55**, 207 (1984), and refs. 2–6 therein.
6. (*a*) R.B. Fearing, E.N. Walsh, J.J. Menn, and A.H. Freiberg. J. Agr. Food Chem. **17**, 1261 (1969); (*b*) D.A. Wustner, J. Desmarchelier, and T.R. Fukuto. Life Sci. **11**, 583 (1972); (*c*) Y. Miyata, Y. Takahashi, and H. Ando. Kag. Keis. Kenkyusho Hok. Hokagaku-hen, **41**, 159 (1988); Chem. Abst. 112:92 231; (*d*) N.K. Roy. Pesticides, 1989–90, 13 (1990); Chem. Abst. 115:273 431.
7. (*a*) L. Malatesta and R. Pizzotti. Chim. e Ind. **27**, 6 (1945); (*b*) L. Malatesta and R. Pizzotti. Gazzo. Chim. Ital. **76**, 167 (1946); (*c*) P.S. Shetty, P. Jose, and Q. Fernando. J. Chem. Soc. Commun. 788 (1968); (*d*) H. Hartung. Z. Chem. **7**, 241 (1967); (*e*) J.P. Fackler, Jr. and L.D. Thompson, Jr. Inorg. Chim. Acta, **48**, 45 (1981).
8. M. Arca, A. Cornia, F.A. Devillanova, A.C. Fabretti, F. Isaia, V. Lippolis, and G. Verani. Inorg. Chim. Acta, **262**, 81 (1997).
9. M. Thorsen, T.P. Andersen, U. Pedersen, B. Yde, S.-O. Lawesson, and H.F. Hansen. Tetrahedron, **41**, 5633 (1985).
10. M. Arca, F. Demartin, F.A. Devillanova, A. Garau, F. Isaia, F. Lelj, V. Lippolis, S. Pedraglio, and G. Verani. J. Chem. Soc. Dalton Trans. 3731 (1998).
11. M.C. Aragoni, M. Arca, F. Demartin, F.A. Devillanova, A. Garau, F. Isaia, F. Lelj, V. Lippolis, and G. Verani. J. Am. Chem. Soc. **121**, 7098 (1999).
12. M.C. Aragoni, M. Arca, F. Demartin, F.A. Devillanova, C. Graiff, F. Isaia, V. Lippolis, A. Tirpicchio, and G. Verani. Eur. J. Chem. **10**, 2239 (2000).
13. J. Labanowsky and J. Andzelm. Density functional methods in chemistry. Springer–Verlag, New York. 1991.
14. C. Adamo and F. Lelj. J. Chem. Phys. **103**, 10605 (1995).
15. C. Daul. Int. J. Quantum Chem. **52**, 867 (1994).
16. J.P. Fackler, Jr. and L.D. Thompson, Jr. Inorg. Chim. Acta, **48**, 45 (1981).
17. H. Hartung. Z. Chem. **6**, 241 (1967).
18. G. Rauhut and P. Pulay. J. Phys. Chem. **99**, 3093 (1995).
19. Gaussian 98 (Revision A.7). M.J. Frisch, G.W. Trucks, H.B. Schlegel, G.E. Scuseria, M.A. Robb, J.R. Cheeseman, V.G. Zakrzewski, J.A. Montgomery, Jr. R.E. Stratmann, J.C. Burant, S. Dapprich, J.M. Millam, A.D. Daniels, K.N. Kudin, M.C. Strain, O. Farkas, J. Tomasi, V. Barone, M. Cossi, R. Cammi, B. Mennucci, C. Pomelli, C. Adamo, S. Clifford, J. Ochterski, G.A. Petersson, P.Y. Ayala, Q. Cui, K. Morokuma, D.K. Malick, A.D. Rabuck, K. Raghavachari, J.B. Foresman, J. Cioslowski, J.V. Ortiz, A.G. Baboul, B.B. Stefanov, G. Liu, A. Liashenko, P. Piskorz, I. Komaromi, R. Gomperts, R.L. Martin, D.J. Fox, T. Keith, M.A. Al-Laham, C.Y. Peng, A. Nanayakkara, C. Gonzalez, M. Challacombe, P.M.W. Gill, B. Johnson, W. Chen, M.W. Wong, J.L. Andres, C. Gonzalez, M. Head-Gordon, E.S. Replogle, and J.A. Pople. Gaussian, Inc. Pittsburgh, PA. 1998.
20. A.D. Becke. J. Chem. Phys. **98**, 1372 (1993).
21. A.D. Becke. J. Chem. Phys. **98**, 5648 (1993).
22. C. Lee, W. Yang, and R.G. Parr. Phys. Rev. B, **37**, 785 (1988).
23. (*a*) P.C. Hariharan and J.A. Pople. Theor. Chim. Acta, **28**, 213 (1973); (*b*) M.M. Francl, W.J. Petro, W.J. Hehre, J.S. Binkley, M.S. Gordon, D.J. DeFrees, and J.A. Pople. J. Chem. Phys. **77**, 3654 (1982); (*c*) V. Rassolov, J.A. Pople, M. Ratner, and T.L. Windus. J. Chem. Phys. **109**, 1223 (1998).
24. G. Schaftenaar and J.H. Noordik. Molden 3.6: a pre- and post-processing program for molecular and electronic structure. Comp.-Aided Mol. Design, **14**, 123 (2000).
25. A.D. Becke. Phys. Rev. A, **38**, 3098 (1988).
26. C. Lee, W. Yang, and R.G. Parr. Phys. Rev. B, **37**, 785 (1988).
27. J.P. Perdew and Y. Wang. Phys Rev B, **45**, 13244 (1992).
28. R. Hoffmann and W.N. Libscomb. J. Chem. Phys. **36**, 2179 (1962).
29. C. Mealli and D.M. Proserpio. J. Chem. Educ. **67**, 399 (1990).
30. H. Fujimoto and R. Hoffmann. J. Phys. Chem. **78**, 1167 (1974).
31. C. Lensch, W. Clegg, and G.M. Sheldrick. J. Chem. Soc. Dalton Trans. 723 (1984).